ISSN 0021-3640, JETP Letters, 2023, Vol. 118, No. 11, pp. 867–874. © The Author(s), 2023. This article is an open access publication.
Russian Text © The Author(s), 2023, published in Pis'ma v Zhurnal Eksperimental'noi i Teoreticheskoi Fiziki, 2023, Vol. 118, No. 11, pp. 860–868.

CONDENSED MATTER

Simultaneous Observation of the Cyclotron Resonances of Electrons and Holes in a HgTe/CdHgTe Double Quantum Well under "Optical Gate" Effect

L. S. Bovkun[a,b], S. S. Krishtopenko[c,d], V. Ya. Aleshkin[b], N. N. Mikhailov[e], S. A. Dvoretsky[e], F. Teppe[c], M. Orlita[a], V. I. Gavrilenko[b], and A. V. Ikonnikov[d,*]

[a] *Laboratoire National des Champs Magnétiques Intenses, CNRS-UGA-EMFL-UPS-INSA, FR-38042 Grenoble, France*
[b] *Institute for Physics of Microstructures, Russian Academy of Sciences, Nizhny Novgorod, 603950 Russia*
[c] *Laboratoire Charles Coulomb, UMR CNRS 5221, Université de Montpellier, Montpellier, 34095 France*
[d] *Faculty of Physics, Moscow State University, Moscow, 119991 Russia*
[e] *Rzhanov Institute of Semiconductor Physics, Siberian Branch, Russian Academy of Sciences, Novosibirsk, 630090 Russia*
**e-mail: antikon@physics.msu.ru*

Received October 13, 2023; revised November 3, 2023; accepted November 7, 2023

Spectral studies of the photoconductivity in the temperature range of $T = 5–70$ K, as well as studies of the magneto-absorption and magnetotransport at $T = 4.2$ K, have been performed in a HgTe/CdHgTe heterostructure with a double quantum well under an "optical gate" effect. Studies of magneto-absorption spectra under the controlled optical exposure have made it possible to observe absorption lines caused by both the cyclotron resonances of electrons and holes simultaneously. The coexistence of electrons and holes in the HgTe/CdHgTe double quantum well with a relatively large bandgap (~80 meV) indicates the appearance of a strongly inhomogeneous light-induced distribution of charge carriers in the plane of the structure. Experimental results obtained clearly demonstrate disadvantages of the control of the Fermi level positions in heterostructures with HgTe/CdHgTe quantum wells by means of the optical gate.

DOI: 10.1134/S0021364023603536

1. INTRODUCTION

HgTe/CdHgTe quantum wells (QWs) demonstrate an enormous variety of physical properties that stem primarily to the qualitative rearrangement of the band structure under the variation of the thickness of QWs [1–3]: from a trivial insulator through the system of two-dimensional (2D) massless Dirac fermions [4–10] to a 2D topological insulator [11–13] and further through a 2D semimetal [14–17] to a three-dimensional (3D) topological insulator [18, 19]. HgTe double quantum wells (DQWs) have an even greater variety of phase states: in addition to the states listed above, they allow the "bilayer graphene" and "double inversion" states [20]. The band gap in the former case can be varied by an electric field, and the latter system can be considered as a higher-order topological insulator [21].

Variety of topological phases, as well as the possibility of affecting the value of the band gap by the applied electric field, provides potentially wide possibility of applications of HgTe/CdHgTe DQWs in electronics and optoelectronics. The possibility of controlling the position of the Fermi level, as well as the concentration and type of charge carriers, is a key property to use HgTe/CdHgTe DQWs in real devices. In particular, to use quantized conductivities observed in the topological insulator phase [22], the Fermi level must be located in the band gap of bulk states. The position of the Fermi level in HgTe/CdHgTe DQWs is usually controlled by fabricating electric gate structures [23–25]. However, such a fabrication is technologically complex, particularly in the case of small (≤1 μm) structures or large (≥ several millimeters) gates.

A simpler alternative method of changing the position of the Fermi level in structures with HgTe/CdHgTe QWs is based on the persistent photoconductivity effect [26–28]. This method is called the "optical gate" [29, 30] or "optical doping" [8, 31]. The optical gate effect is a light-induced change in the conductivity of the 2D system and the subsequent holding of this new state after the end of illumination. The optical gate effect in most 2D systems can lead only to an increase or a decrease in the charge carrier concentration (see, e.g., [32–37]), but the type of conductivity can also change in some systems, e.g., HgTe/CdHgTe QWs [10, 27, 38]. In particular, as found in [10], the controlled illumination of single HgTe/CdHgTe gap-

less QWs by green light changes the type of charge carriers from holes to electrons. The "identity" of the electric and optical gates was in fact demonstrated in [10]. The illumination-induced change in the type of conductivity was also detected in the HgTe/CdHgTe DQWs with a band gap of about 80 meV [38]. However, only the "dark" state with the hole conductivity and the "illuminated" state with the electron conductivity that is due to long-term illumination were studied in [38]. The possibility of a *reversible* change in the type of conductivity in HgTe/CdHgTe DQWs irradiated by light with various photon energies was also demonstrated [27]. All these allow one to hope that the use of the optical gate in the structure with HgTe/CdHgTe QWs will make it possible to control the position of the Fermi level, in particular, to fix it at the charge neutrality point by varying the duration of illumination.

The aim of this work is to determine the behavior of the Fermi level under controlled optical action on structures with HgTe/CdHgTe DQWs with a relatively large band gap. We chose this sample because a similar sample had already demonstrated a change in the sign of the conductivity under the optical gate effect [38], and average values of the band gap (~80 meV) in the chosen structure should significantly exceed the scale of fluctuations of the bandgap. One of the most direct methods of studying the band structure of bulk materials and heterostructures with QWs is magneto-absorption spectroscopy, which allows for the direct reconstruction of the band structure in the case of low magnetic fields (cyclotron resonance) at various positions of the Fermi level [7, 17]. The band structure can be reconstructed by comparing theoretical calculations of transitions between Landau levels with the experimentally observed features of magneto-absorption spectra measured in quantized magnetic fields [6, 7, 15, 38–46]. Additional information on the band gap and on its temperature dependence can also be obtained from photoconductivity spectra [47, 48].

In this work, we study magneto-absorption and photoconductivity spectra, as well as transport properties in HgTe/CdHgTe DQWs under the optical gate effect. First, comparing experimental results with model calculations with an eight-band Kane Hamiltonian, we refine the widths of the layers of HgTe/CdHgTe DQW. Second, we study the magneto-absorption and the Hall effect in the HgTe/CdHgTe DQW exposed to the controlled optical illumination by blue light at low temperatures. It is shown that successive illumination results in a change from hole charge carriers to electron ones, which is manifested in both transport measurements and magneto-absorption spectra. At the same time, absorption lines caused by both the electron and hole cyclotron resonances are surprisingly observed in magneto-absorption spectra at a certain intermediate illumination. The coexistence of electrons and holes in the sample with a relatively large band gap of about 80 meV indicates the appearance of a strongly inhomogeneous light-induced distribution of charge carriers in the plane of the sample under the optical gate effect.

2. METHODS

The studied structure was grown by molecular beam epitaxy (MBE) on a 400-μm-thick GaAs (013) semi-insulating substrate [49, 50]. A buffer consisting of a 30-nm ZnTe layer and a 5-μm-thick CdTe relaxed layer was grown on the substrate. The active part of the structure consisted of the 30-nm bottom $Cd_xHg_{1-x}Te$ barrier, two HgTe QWs with the thickness d separated by a $Cd_xHg_{1-x}Te$ tunnel barrier with the thickness t, and the 30-nm top $Cd_xHg_{1-x}Te$ barrier. A 40-nm-thick CdTe cap layer was grown above the entire structure. The structure was not intentionally doped. The nominal growth parameters of the structure were $x = 0.64$, $d = 4.5$ nm, and $t = 3.0$ nm.

Photoconductivity spectra were studied in the temperature range of 5–70 K using a Bruker Vertex 70v Fourier-transform spectrometer. To this end, strip contacts were deposited on the edges of the 4 × 5-mm sample. We used a Globar as a radiation source and a Mylar Multilayer beamsplitter. The sample was placed in an Oxford Instruments OptistatCF helium-flow cryostat, which had polypropylene and Mylar windows and was placed in the spectrometer so that the sample was in the focus of the radiation beam. A cold black polyethylene filter was placed in front of the sample. The spectral characteristics of all used optical elements and filters allow one to record photoconductivity spectra in the range of 4–120 meV, except for an opaque region of the beamsplitter of 87–92 meV. A spectral resolution was set to 1 meV.

Magnetoabsorption spectra were recorded at Laboratoire National des Champs Magnétiques Intenses (LNCMI-G, Grenoble, France) with a Bruker 80v Fourier-transform spectrometer in static magnetic fields up 11 T and at the Moscow State University with terahertz quantum-cascade lasers under the variation of the magnetic field up to 4.5 T at a temperature of $T = 4.2$ K. In the former case, 5 × 5-mm samples were placed in a waveguide insert in the center of a superconducting solenoid in liquid helium. A light-emitting diode placed near the sample allowed the controlled illumination of the sample by blue light. A black polyethylene or ZnSe filter was placed between the insert and the Fourier-transform spectrometer. Studies were carried out in the Faraday geometry; i.e., the axis of growth of the HgTe/CdHgTe DQW was parallel to the magnetic field and the direction of propagation of radiation. We used a Globar as a radiation source and a Mylar Multilayer or KBr beamsplitter. Radiation transmitted through the sample was detected by a composite silicon bolometer. A signal from the bolometer was fed to the analog-to-digital converter of the Fourier-transform spectrometer. Spectra obtained

with a spectral resolution of 0.5 meV were normalized to the spectrum in zero magnetic field.

Measurements at the Moscow State University with terahertz quantum-cascade lasers with frequencies of 2.27 and 3.0 THz, which were used as sources of monochromatic radiation (pulse duration of 10–20 μs and a repetition frequency of 19 Hz). Magnetoabsorption spectra were also recorded in the Faraday geometry. The sample could also be illuminated by blue light. A Ge:Ga crystal was used as a detector. Radiation transmitted through the sample was received by the detector, a signal from which was amplified and fed on a boxcar averager. The Hall effect was simultaneously measured, which allowed the determination of the concentration and type of charge carriers. To this end, point indium contacts were sealed on 4 × 5-mm samples in the Hall geometry.

To calculate the band structure, Landau levels, and transition matrix elements in the studied sample, we used the eight-band Kane Hamiltonian in the axial approximation for structures with the (013) orientation [6, 46] and took into account the built-in deformation caused by the difference between the lattice constants of the CdTe buffer, $Cd_xHg_{1-x}Te$ barriers, and HgTe QWs. The plane-wave expansion was used to determine the coordinate dependences of the envelopes of the function in the direction perpendicular to the plane of QWs. The influence of the magnetic field was taken into account by means of the Peierls substitution, and the transverse part of envelope functions was expanded in the wavefunctions of the free electron in a uniform magnetic field. To numerically calculate envelope functions and the corresponding energies of electrons, the structure was considered as a superlattice of weakly coupled quantum wells with the period such that the interaction between them hardly affected the energy spectrum of the system. To describe the effect of the temperature on the band structure of the HgTe/CdHgTe DQW, the temperature dependences of the band gap of HgTe and CdHgTe, valence band offset at the heterointerface, lattice constants of the layers, and elastic constants were taken into account in the eight-band Kane Hamiltonian. The calculation method was described in more detail in [3]. The dependence of the semiclassical cyclotron mass on the charge carrier concentration was determined from the dispersion relation of charge carriers in a particular band.

3. RESULTS AND DISCUSSION

3.1. Band Structure Parameters

According to the calculations reported in [20], the studied structure should have a normal band structure (energies of all electron subbands are greater than any hole subband). This is also confirmed by our experimental studies. Figure 1a presents photoconductivity spectra measured at various temperatures. It is seen that the long wavelength cut-off of the photoconductivity is blueshifted with increasing temperature. This certainly indicates that the studied structure has the normal band structure [48]. Furthermore, these spectra allow one to estimate the band gap E_g as (76 ± 3) meV at low temperatures. This value is close to 77 meV presented in [38] for this structure and is significantly larger than a value of 31 meV determined from calculations of the band structure with nominal growth parameters. All these show that the real parameters of the DQW layers noticeably differ from the growth parameters determined by ellipsometry.

Magneto-optical studies also confirmed the made assumption. Figure 1b shows the magneto-absorption false-color map obtained with the maximum illumination by blue light (Fermi level in the conduction band). Figure 1c presents the magneto-absorption spectrum recorded in a magnetic field of 6.75 T. Two main lines α and β_1 are primarily seen in the spectra. The former line corresponds to an intraband transition, and its extrapolation to zero magnetic field gives zero energy. The latter line corresponds to interband (one or several) transitions, and its extrapolation to zero magnetic field provides a nonzero energy (see, e.g., [42, 48]), which makes it possible to estimate the band gap as (76 ± 2) meV, coinciding with the value estimated from photoconductivity data.

As mentioned above, the calculations of the band structure using the nominal parameters of the layers give a band gap of 31 meV; consequently, the adequate theoretical description of observed magneto-absorption spectra requires the correction of the parameters of the DQW used in calculations. A similar correction was also used in [38, 41], where magneto-absorption was studied in HgTe DQW grown in the same MBE setup. Since our sample was grown in the same growth cycle as the structures with the HgTe/CdHgTe DQW studied in [41], when correcting the parameters of DQWs, we also reduced the width of the QWs d and the tunnel barrier t, holding the relative content of Cd in barriers. Nevertheless, to achieve good agreement between calculations and experimental data, it was also necessary to enable a nonzero content of Cd y in layers of $Hg_{1-y}Cd_yTe$ QWs. The best agreement with experimental data was achieved at the parameters $x = 0.64$, $y = 0.02$, $d = 4.0$ nm, and $t = 2.8$ nm (see Fig. 1b). At these parameters of the sample, the line α in magneto-absorption spectra corresponds to the intraband $0 \to 1$ transition in the conduction band, and the line β_1 corresponds to the interband $-2 \to -1$ and $-1 \to 0$ transitions (see Fig. 1d). Moreover, theoretical calculations with these parameters well reproduce not only the behavior of other lines in magneto-absorption spectra under the variation of the magnetic field (see Fig. 1b) but also the temperature dependence of the cut-off of the photoconductivity (see the inset of Fig. 1a).

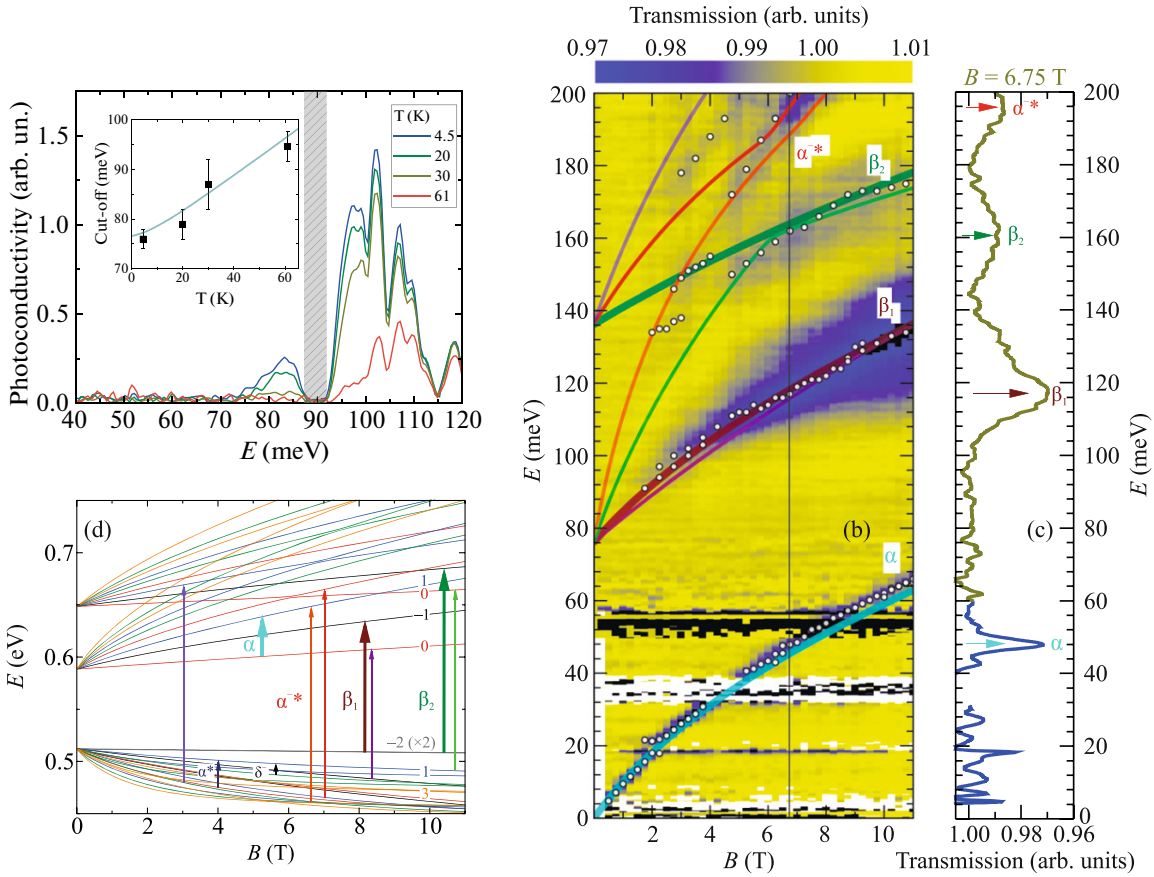

Fig. 1. (Color online) (a) Photoconductivity spectra of the HgTe/CdHgTe DQW at various temperatures. The gray band is the opaque region of the used Mylar Multilayer beamsplitter. The inset shows (squares with error bars) the temperature dependence of the cut-off of the photoconductivity and the calculated temperature dependence of the band gap. (b) Magneto-absorption false-color map and (c) the magneto-absorption spectrum of the HgTe/CdHgTe DQW. Darker regions correspond to stronger absorption. Circles are data from [38]. Lines are transitions between Landau levels calculated with corrected parameters. The map and spectrum are composed from two sets of measurements with various filters and beamsplitters: the black polyethylene filter and the Mylar Multilayer beamsplitter were used in measurements for energies below 60 meV, and the ZnSe filter and the KBr beamsplitter were applied for energies above 60 meV. The vertical solid straight line in panel (b) marks a magnetic field of 6.75 T, for which the spectrum is shown in panel (c). (d) Landau levels that are calculated with the corrected parameters of the layers of the DQW. Levels enumerated according to [6, 39, 46]. Arrows mark observed transitions in notation from [39, 41, 42, 46]). The upper −2 Landau level of the valence band is doubly degenerate due to the symmetry of the double quantum well.

3.2. Magneto-Absorption at Various Durations of Optical Illumination

After the more accurate determination of the real parameters of the sample layers, it was possible to examine subtle effects, in particular, the transformation of magneto-absorption lines during the transition from hole to electronic type of conductivity when using the optical gate. Figure 2 presents magneto-absorption spectra obtained under dark conditions and after the controlled illumination of samples by blue light. As seen in Fig. 2a, magneto-absorption spectra recorded under dark conditions exhibit three main lines, two of them below 30 meV (α^* and δ^-) and one above 100 meV (β_1). As mentioned above, the last line corresponds to the interband $-2 \rightarrow -1$ and $-1 \rightarrow 0$ transitions (see Fig. 1d). Calculations of transition matrix elements show that the leading contribution comes from the $-2 \rightarrow -1$ transition. Interband transitions are much more sensitive than intraband transitions to fluctuations of the parameters of the structures (and to related fluctuations of the bandgap). As a result, the width of the line β_1 is noticeably larger than the widths of lines α, α^*, and δ^- (see Figs. 1c and 2). The last two lines are obviously due to intraband transitions because their energy in the entire magnetic field range does not exceed the bandgap (76 meV).

Measurements of the Hall effect show that the structure under dark conditions has the hole conductivity (see line *1* in Fig. 3a). In addition, it is seen in Fig. 2a that a magnetic field of about 5–6 T, above which the line β_1 appears, coincides with the magnetic

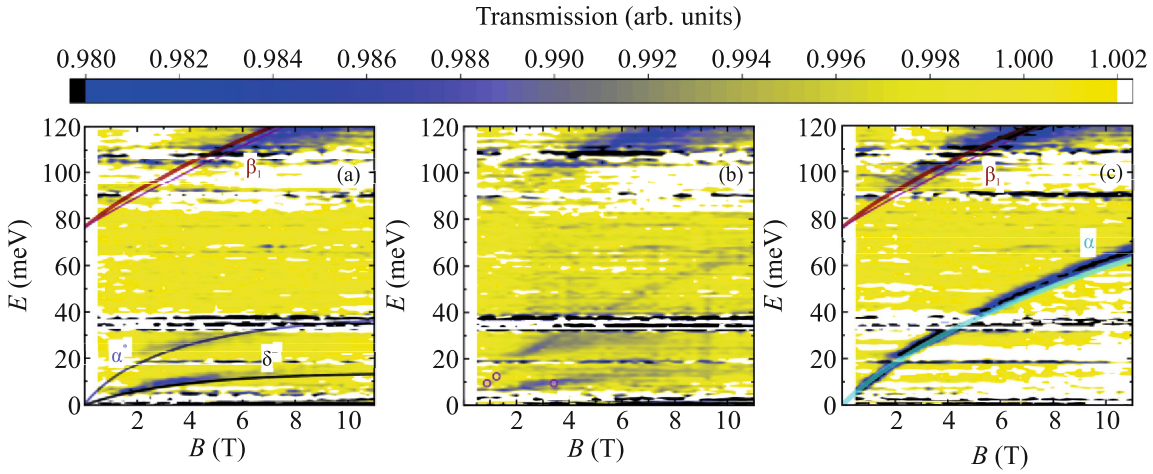

Fig. 2. (Color online) Magneto-absorption false-color maps of the HgTe/CdHgTe double quantum well obtained (a) under dark conditions, (b) after the short-term (<1 s) illumination by blue light, and (c) after the long-term (>10 s) illumination by blue light. Darker regions correspond to stronger absorption. Color lines correspond to the calculated transitions between Landau levels. The black polyethylene filter and the Mylar Multilayer beamsplitter were used in the measurements of the spectra. Empty circles in panel (b) mark the positions of magneto-absorption lines measured by quantum-cascade lasers. Panel (c) partially repeats Fig. 1b.

field in which the intensities of the lines α^* and δ^- drop significantly. Since the leading contribution to the line β_1 comes from the $-2 \to -1$ transition, the line β_1 can be attributed to the appearance of electrons on one of the -2 levels (see Fig. 1d), which corresponds to the filling factor $\nu = 2$ (the corresponding hole concentration is $\sim 2.7 \times 10^{11}$ cm^{-2}). In this case, the attenuation of the lines α^* and δ^- will be due to the complete filling of the top 1 level in the valence band with electrons (see Fig. 1d). Therefore, the lines α^* and δ^- can be attributed to the $0 \to 1$ and $2 \to 1$ intraband transitions in the valence band, respectively (see Fig. 1d). Some discrepancy between the positions of the line α^* and the $0 \to 1$ transition, as well as an incomplete disappearance of the lines α^* and δ^- in fields above 5–6 T, can be explained by the "mixing" of closely located Landau levels due to the symmetry lowering [42, 45], which was disregarded in this work. The charge carrier concentrations obtained from transport measurements slightly differ from those at which the filling factors of Landau levels discussed above are reached. For the dark case (see line *1* in Fig. 3a), the hole concentration determined from the slope of the Hall curve is as low as 0.8×10^{11} cm^{-2}. This situation is most probably due to the pinning of the Fermi level at the side maximum of the valence band, where holes do not contribute to the quantum Hall effect [25] and, as a result, the concentration in transport measurements in low magnetic fields is lower.

Optical illumination qualitatively changes magneto-absorption spectra due to the persistent photoconductivity effect, which is pronounced in HgTe/CdHgTe DQWs [27]. In particular, after the long-term (>10 s) illumination by blue light (see Fig. 2c), the lines α^* and δ^- are replaced by the single intense line α whose position is in excellent agreement with the $0 \to 1$ transition in the conduction band, which corresponds to electron cyclotron resonance in the quantum limit. In low magnetic fields <2 T, the position of this line linearly depends on the magnetic field and corresponds to the "classical" electron cyclotron resonance line for a cyclotron mass of $0.0127m_0$. From the calculated dependence of the cyclotron mass on the carrier concentration in the conduction band (see the inset of Fig. 3b), the electron concentration can be estimated as 0.45×10^{11} cm^{-2}. This value is close to the value obtained from the concentration estimated by the position of the plateau for the $\nu = 1$ quantum Hall effect (see line *3* in Fig. 3a). The observation of the electron cyclotron resonance lines after optical illumination is in good agreement with transport measurements (see Fig. 3a), which confirm the illumination-induced change in the type of conductivity (the signs of the Hall effect for lines *1* and *3* in Fig. 3a are opposite).

Of the most interest are magneto-absorption spectra in the HgTe/CdHgTe DQW obtained after the short-term (<1 s) illumination by blue light (see Fig. 2c). The magneto-absorption map in this case qualitatively is a superposition of maps obtained in the dark and maximum illumination cases. Indeed, as seen in Fig. 2b, magneto-absorption spectra simultaneously include the lines α^* and δ^-, which is due to the hole cyclotron resonance, and the electron cyclotron resonance line α. Electron and hole cyclotron resonance lines are also simultaneously observed in magneto-absorption spectra obtained with quantum-cas-

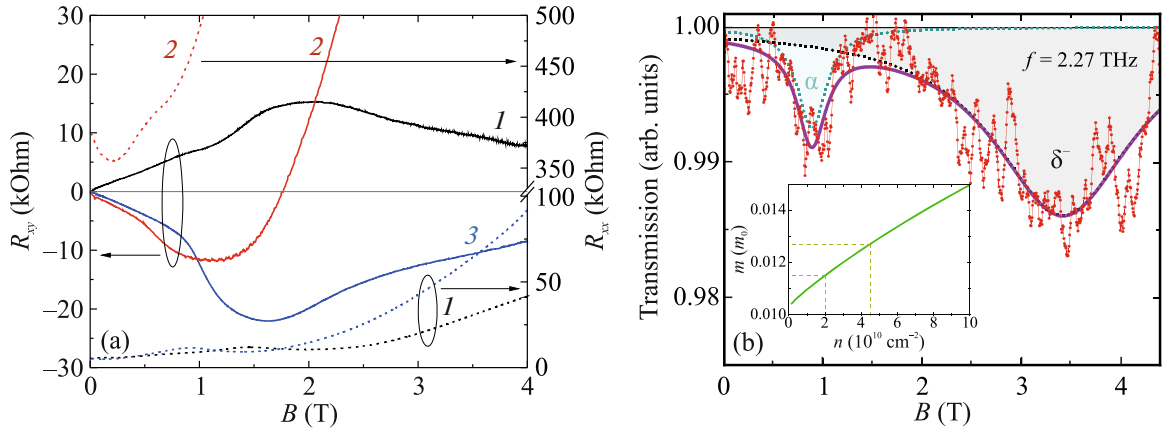

Fig. 3. (Color online) (a) Magnetic field dependences of the (solid lines) Hall, R_{xy}, and (dashed lines) longitudinal, R_{xx}, resistances measured (*1*) under dark conditions, (*2*) after the short-term (<1 s) illumination by blue light, and (*3*) after the long-term (>10 s) illumination by blue light. Positive R_{xy} values correspond to the hole conductivity. (b) Magneto-absorption spectrum of the HgTe/CdHgTe double quantum well measured by quantum-cascade lasers at a fixed radiation frequency under the variation of the magnetic field after the short-term illumination by blue light, and the approximation of the spectrum by two Lorentzians. The spectrum exhibits the lines α and δ^- corresponding to the electron and hole cyclotron resonances, respectively. The inset shows the cyclotron mass versus the electron concentration in the lower subband of the conduction band. Dashed lines are the masses determined from magneto-absorption spectra in low magnetic fields and the corresponding electron concentrations.

cade lasers at a fixed frequency under the variation of the magnetic field (see Fig. 3b). We note that the appearance of the line β_1 and the disappearance of the lines α^* and δ^- in Fig. 2b occur in slightly lower magnetic fields (about 4–5 T) than those in the dark case (see Fig. 2a), which indicates a lower hole concentration (~2.0×10^{11} cm^{-2}). At the same time, the classical electron cyclotron resonance gives the mass $0.0115m_0$, which corresponds to an electron concentration of 0.2×10^{11} cm^{-2} (see the inset of Fig. 3b). We emphasize that the electron and hole cyclotron resonance lines can be simultaneously observed for several hours after the removal of optical illumination.

The reported experimental results on the simultaneous detection of electron and hole absorption lines in the HgTe/CdHgTe DQW with a relatively large band gap are surprising and indicate the appearance of a strongly inhomogeneous distribution of charge carriers in the plane of the structure under the optical gate effect. To the best of our knowledge, such inhomogeneities in the charge carrier distribution under persistent photoconductivity conditions were observed for the first time in the measurement of oscillation beatings of the longitudinal magnetoresistance (Shubnikov–de Haas oscillations) in InAs/AlSb QW heterostructures [51]. In particular, it was shown that the appearance of two frequencies in oscillations of the magnetoresistance directly depends on the illumination time of the sample: oscillation beatings were observed only at a certain illumination dose and were not observed at a high illumination dose. The appearance of beatings of Shubnikov–de Haas oscillations was explained in [51] by the formation of regions with different charge carrier concentration on the path of the current in the Hall geometry. In our case, the short-term illumination of the sample with the HgTe/CdHgTe DQW apparently results in the inhomogeneous distribution of charge carriers under the optical gate effect.

Since the type of conductivity in the HgTe/CdHgTe DQW also depends on the illumination time, simultaneous appearance of electrons and holes at a certain illumination dose due to the formation of the photoinduced inhomogeneous charge distribution seems reasonable. This is a direct analogy with the appearance of beatings of Shubnikov–de Haas oscillations in InAs/AlSb QWs at a certain illumination dose [51]. However, the coexistence of electrons and holes spatially separated in the plane of the sample with the HgTe/CdHgTe DQW leads to a pronounced nonlinearity of the Hall resistance R_{xy} instead of oscillation beatings (see line *2* in Fig. 3a). The scale of such a nonequilibrium spatial separation of electrons and holes in the plane of the DQW should obviously be much larger than the spatial scale of overlapping of their wavefunctions to exclude the possibility of their recombination. We note that the described mechanism of coexistence of electrons and holes under persistent photoconductivity conditions is not a unique property of the HgTe/CdHgTe DQW. It can be manifested in any heterostructures with QWs with a normal or inverted band structure, where the persistent photoconductivity effect leads to a change in the type of conductivity. Unfortunately, a theory that allows one to quantitatively describe the formation of the inhomogeneous distribution of charge carriers

under the optical gate effect depending on the optical illumination time is currently absent. However, our experimental results have already demonstrated demerits of the optical gate control of the position of the Fermi level in heterostructures with HgTe/CdHgTe QWs.

ACKNOWLEDGMENTS

The authors are grateful to Laboratoire National des Champs Magnétiques Intenses (LNCMI-G), member of the European Magnetic Field Laboratory for support.

FUNDING

This work was supported by the Russian Science Foundation (project no. 22-22-00382).

CONFLICT OF INTEREST

The authors of this work declare that they have no conflicts of interest.

REFERENCES

1. L. G. Gerchikov and A. Subashiev, Phys. Status Solidi B **160**, 443 (1990).
2. B. A. Bernevig, T. L. Hughes, and S. C. Zhang, Science (Washington, DC, U. S.) **314**, 1757 (2006).
3. S. S. Krishtopenko, I. Yahniuk, D. B. But, V. I. Gavrilenko, W. Knap, and F. Teppe, Phys. Rev. B **94**, 245402 (2016).
4. B. Buttner, C. X. Liu, G. Tkachov, E. G. Novik, C. Brune, H. Buhmann, E. M. Hankiewicz, P. Recher, B. Trauzettel, S. C. Zhang, and L. W. Molenkamp, Nat. Phys. **7**, 418 (2011).
5. Z. D. Kvon, S. N. Danilov, D. A. Kozlov, K. Tsot, N. N. Mikhailov, S. A. Dvoretskii, and S. D. Ganichev, JETP Lett. **94**, 816 (2011).
6. M. Zholudev, F. Teppe, M. Orlita, et al., Phys. Rev. B **86**, 205420 (2012).
7. J. Ludwig, Yu. B. Vasilyev, N. N. Mikhailov, J. M. Poumirol, Z. Jiang, O. Vafek, and D. Smirnov, Phys. Rev. B **89**, 241406(R) (2014).
8. V. Dziom, A. Shuvaev, N. N. Mikhailov, and A. Pimenov, 2D Mater. **4**, 024005 (2017).
9. M. Marcinkiewicz, S. Ruffenach, S. S. Krishtopenko, et al., Phys. Rev. B **96**, 035405 (2017).
10. A. Shuvaev, V. Dziom, J. Gospodarič, E. G. Novik, A. A. Dobretsova, N. N. Mikhailov, Z. D. Kvon, and A. Pimenov, Nanomaterials **12**, 2492 (2022).
11. M. König, S. Wiedmann, C. Brüne, A. Roth, H. Buhmann, L. W. Molenkamp, X. L. Qi, and S. C. Zhang, Science (Washington, DC, U. S.) **318**, 766 (2007).
12. A. Roth, C. Brüne, H. Buhmann, L. W. Molenkamp, J. Maciejko, X. L. Qi, and S. C. Zhang, Science (Washington, DC, U. S.) **325**, 294 (2009).
13. E. B. Olshanetsky, Z. D. Kvon, G. M. Gusev, A. D. Levin, O. E. Raichev, N. N. Mikhailov, and S. A. Dvoretsky, Phys. Rev. Lett. **114**, 126802 (2015).
14. Z. D. Kvon, E. B. Olshanetsky, D. A. Kozlov, N. N. Mikhailov, and S. A. Dvoretskii, JETP Lett. **87**, 502 (2008).
15. M. S. Zholudev, A. V. Ikonnikov, F. Teppe, M. Orlita, K. V. Maremyanin, K. E. Spirin, V. I. Gavrilenko, W. Knap, S. A. Dvoretskiy, and N. N. Mihailov, Nanoscale Res. Lett **7**, 534 (2012).
16. A. A. Greshnov, Yu. B. Vasil'ev, N. N. Mikhailov, G. Yu. Vasil'eva, and D. Smirnov, JETP Lett. **97**, 102 (2013).
17. J. Gospodarič, A. Shuvaev, N. N. Mikhailov, Z. D. Kvon, E. G. Novik, and A. Pimenov, Phys. Rev. B **104**, 115307 (2021).
18. C. Brüne, C. X. Liu, E. G. Novik, E. M. Hankiewicz, H. Buhmann, Y. L. Chen, X. L. Qi, Z. X. Shen, S. C. Zhang, and L. W. Molenkamp, Phys. Rev. Lett. **106**, 126803 (2011).
19. D. A. Kozlov, Z. D. Kvon, E. B. Olshanetsky, N. N. Mikhailov, S. A. Dvoretsky, and D. Weiss, Phys. Rev. Lett. **112**, 196801 (2014).
20. S. S. Krishtopenko, W. Knap, and F. Teppe, Sci. Rep. **6**, 30755 (2016).
21. S. S. Krishtopenko, Sci. Rep. **11**, 21060 (2021).
22. M. Z. Hasan and C. L. Kane, Rev. Mod. Phys. **82**, 3045 (2010).
23. G. M. Gusev, E. B. Olshanetsky, F. G. G. Hernandez, O. E. Raichev, N. N. Mikhailov, and S. A. Dvoretsky, Phys. Rev. B **101**, 241302(R) (2020).
24. G. M. Gusev, E. B. Olshanetsky, F. G. G. Hernandez, O. E. Raichev, N. N. Mikhailov, and S. A. Dvoretsky, Phys. Rev. B **103**, 035302 (2021).
25. M. V. Yakunin, S. S. Krishtopenko, W. Desrat, S. M. Podgornykh, M. R. Popov, V. N. Neverov, S. A. Dvoretsky, N. N. Mikhailov, F. Teppe, and B. Jouault, Phys. Rev. B **102**, 165305 (2020).
26. K. E. Spirin, D. M. Gaponova, K. V. Marem'yanin, V. V. Rumyantsev, V. I. Gavrilenko, N. N. Mikhailov, and S. A. Dvoretsky, Semiconductors **52**, 1586 (2018).
27. I. Nikolaev, A. Kazakov, K. Drozdov, M. Bannikov, K. Spirin, R. Menshchikov, S. Dvoretsky, N. Mikhailov, D. Khokhlov, and A. Ikonnikov, J. Appl. Phys. **132**, 234301 (2022).

28. M. K. Sotnichuk, A. S. Kazakov, I. D. Nikolaev, K. A. Drozdov, R. V. Menshchikov, S. A. Dvoretsky, N. N. Mikhailov, D. R. Khokhlov, and A. V. Ikonnikov, Photonics **10**, 877 (2023).
29. A. L. Yeats, Y. Pan, A. Richardella, P. J. Mintun, N. Samarth, and D. D. Awschalom, Sci. Adv. **1**, e1500640 (2015).
30. I. D. Nikolaev, T. A. Uaman Svetikova, V. V. Rumyantsev, M. S. Zholudev, D. V. Kozlov, S. V. Morozov, S. A. Dvoretsky, N. N. Mikhailov, V. I. Gavrilenko, and A. V. Ikonnikov, JETP Lett. **111**, 575 (2020).
31. C. Zoth, P. Olbrich, P. Vierling, K.-M. Dantscher, V. V. Bel'kov, M. A. Semina, M. M. Glazov, L. E. Golub, D. A. Kozlov, Z. D. Kvon, N. N. Mikhailov, S. A. Dvoretsky, and S. D. Ganichev, Phys. Rev. B **90**, 205415 (2014).
32. A. Kastalsky and J. C. M. Hwang, Solid State Commun. **51**, 317 (1984).
33. L. C. Tsai, C. F. Huang, J. C. Fan, Y. H. Chang, and Y. F. Chen, J. Appl. Phys. **84**, 877 (1998).
34. W. C. Wang, L. C. Tsai, J. C. Fan, and Y. F. Chen, J. Appl. Phys. **86**, 3152 (1999).
35. A. S. Chaves and H. Chacham, Appl. Phys. Lett. **66**, 727 (1995).
36. V. Ya. Aleshkin, V. I. Gavrilenko, D. M. Gaponova, A. V. Ikonnikov, K. V. Marem'yanin, S. V. Morozov, Yu. G. Sadof'ev, S. R. Johnson, and Y. H. Zhang, Semiconductors **39**, 22 (2005).
37. K. E. Spirin, K. P. Kalinin, S. S. Krishtopenko, K. V. Maremyanin, V. I. Gavrilenko, and Yu. G. Sadofyev, Semiconductors **46**, 1396 (2012).
38. L. S. Bovkun, S. S. Krishtopenko, A. V. Ikonnikov, V. Ya. Aleshkin, A. M. Kadykov, S. Ruffenach, C. Consejo, F. Teppe, W. Knap, M. Orlita, B. Piot, M. Potemski, N. N. Mikhailov, S. A. Dvoretskii, and V. I. Gavrilenko, Semiconductors **50**, 1532 (2016).
39. M. Schultz, U. Merkt, A. Sonntag, U. Rossler, R. Winkler, T. Colin, P. Helgesen, T. Skauli, and S. Løvold, Phys. Rev. B **57**, 14772 (1998).
40. A. V. Ikonnikov, M. S. Zholudev, K. V. Marem'yanin, K. E. Spirin, A. A. Lastovkin, V. I. Gavrilenko, S. A. Dvoretskii, and N. N. Mikhailov, JETP Lett. **95**, 406 (2012).
41. L. S. Bovkun, A. V. Ikonnikov, V. Ya. Aleshkin, K. V. Maremyanin, N. N. Mikhailov, S. A. Dvoretskii, S. S. Krishtopenko, F. Teppe, B. A. Piot, M. Potemski, M. Orlita, and V. I. Gavrilenko, Opto-Electron. Rev. **27**, 213 (2019).
42. L. S. Bovkun, A. V. Ikonnikov, V. Ya. Aleshkin, K. E. Spirin, V. I. Gavrilenko, N. N. Mikhailov, S. A. Dvoretskii, F. Teppe, B. A. Piot, M. Potemski, and M. Orlita, J. Phys.: Condens. Matter **31**, 145501 (2019).
43. A. V. Ikonnikov, S. S. Krishtopenko, O. Drachenko, et al., Phys. Rev. B **94**, 155421 (2016).
44. L. S. Bovkun, A. V. Ikonnikov, V. Ya. Aleshkin, S. S. Krishtopenko, N. N. Mikhailov, S. A. Dvoretskii, M. Potemski, B. Pio, M. Orlita, and V. I. Gavrilenko, JETP Lett. **108**, 329 (2018).
45. M. S. Zholudev, F. Teppe, S. V. Morozov, M. Orlita, C. Consejo, S. Ruffenach, V. Knap, V. I. Gavrilenko, S. A. Dvoretskii, and N. N. Mikhailov, JETP Lett. **100**, 790 (2014).
46. A. V. Ikonnikov, M. S. Zholudev, K. E. Spirin, et al., Semicond. Sci. Technol. **26**, 125011 (2011).
47. V. V. Rumyantsev, A. V. Ikonnikov, A. V. Antonov, S. V. Morozov, M. S. Zholudev, K. E. Spirin, V. I. Gavrilenko, S. A. Dvoretskii, and N. N. Mikhailov, Semiconductors **47**, 1438 (2013).
48. A. V. Ikonnikov, L. S. Bovkun, V. V. Rumyantsev, S. S. Krishtopenko, V. Ya. Aleshkin, A. M. Kadykov, M. Orlita, M. Potemski, V. I. Gavrilenko, S. V. Morozov, S. A. Dvoretsky, and N. N. Mikhailov, Semiconductors **51**, 1531 (2017).
49. S. Dvoretsky, N. Mikhailov, Y. Sidorov, V. Shvets, S. Danilov, B. Wittman, and S. Ganichev, J. Electron. Mater. **39**, 918 (2010).
50. N. N. Mikhailov, R. N. Smirnov, S. A. Dvoretsky, Y. G. Sidorov, V. A. Shvets, E. V. Spesivtsev, and S. V. Rykhlitski, Int. J. Nanotechnol. **3**, 120 (2006).
51. S. Brosig, K. Ensslin, R. J. Warburton, C. Nguyen, B. Brar, M. Thomas, and H. Kroemer, Phys. Rev. B **60**, R13989(R) (1999).